COMPUTER METHODS AND PROGRAMS IN BIOMEDICINE 122 (2015) 372–383

journal homepage: www.intl.elsevierhealth.com/journals/cmpb

Computer-assisted diagnosis for chronic heart failure by the analysis of their cardiac reserve and heart sound characteristics

Yineng Zheng[a], *Xingming Guo*[a,*], *Jian Qin*[b], *Shouzhong Xiao*[a]

[a] *Key Laboratory of Biorheology Science and Technology, Ministry of Education, College of Bioengineering, Chongqing University, Chongqing 400044, PR China*

[b] *Department of Cardiology, First Affiliated Hospital, Chongqing University of Medical Sciences, Chongqing 400044, PR China*

ARTICLE INFO

Article history:
Received 23 April 2015
Received in revised form
23 August 2015
Accepted 1 September 2015

Keywords:
Heart sound
Cardiac reserve
MF-DFA
MESE
EMD
CHF

ABSTRACT

An innovative computer-assisted diagnosis system for chronic heart failure (CHF) was proposed in this study, based on cardiac reserve (CR) indexes extraction, heart sound hybrid characteristics extraction and intelligent diagnosis model definition. Firstly, the modified wavelet packet-based denoising method was applied to data pre-processing. Then, the CR indexes such as the ratio of diastolic to systolic duration (*D*/*S*) and the amplitude ratio of the first to second heart sound (*S*1/*S*2) were extracted. The feature set consisting of the heart sound characteristics such as multifractal spectrum parameters, the frequency corresponding to the maximum peak of the normalized PSD curve (f_{PSDmax}) and adaptive sub-band energy fraction (*sub_EF*) were calculated based on multifractal detrended fluctuation analysis (MF-DFA), maximum entropy spectra estimation (MESE) and empirical mode decomposition (EMD). Statistical methods such as *t*-test and receiver operating characteristic (ROC) curve analysis were performed to analyze the difference of each parameter between the healthy and CHF patients. Finally, least square support vector machine (LS-SVM) was employed for the implementation of intelligent diagnosis. The result indicates the achieved diagnostic accuracy, sensitivity and specificity of the proposed system are 95.39%, 96.59% and 93.75% for the detection of CHF, respectively. The selected cutoff values of the diagnosis features are $D/S = 1.59$, $S1/S2 = 1.31$, $\Delta\alpha = 1.34$ and $f_{PSDmax} = 22.49$, determined by ROC curve analysis. This study suggests the proposed methodology could provide a technical clue for the CHF point-of-care system design and be a supplement for CHF diagnosis.

1. Introduction

Chronic heart failure (CHF) occurs in the situation that heart loses the ability to pump adequate oxygen-rich blood to meet the need of peripheral tissues and organs of the body. This may cause some symptoms such as shortness of breath, tiredness, irregular heartbeats, etc. Compared to the expensive imageological diagnosis and biochemical analysis, it is of great significance to develop a non-invasive, low-cost and convenient detection method for CHF diagnosis.

* *Corresponding author*. Tel.: +86 23 65112676; fax: +86 23 65102507.
E-mail address: guoxm@cqu.edu.cn (X. Guo).

http://dx.doi.org/10.1016/j.cmpb.2015.09.001
0169-2607/

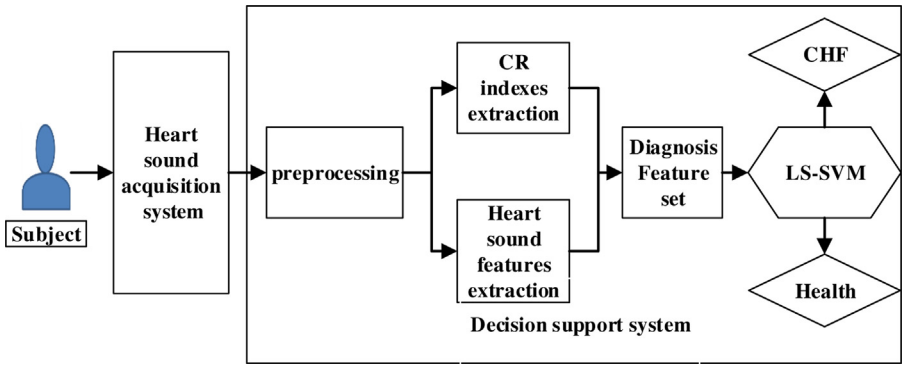

Fig. 1 – The schematic of the computer-assisted diagnosis system for CHF.

Many researchers have devoted themselves to the studies on computer-assisted diagnosis for CHF based on the detection and analysis of Electrocardiograph (ECG). Ivanov et al. [1,2] and Dutta [3] have found there are both a loss of multifractality in heartbeat sequences and ECG of the patients with CHF. The prolongation duration of QRS or wide QRS/T angles could be a predictive indicator of CHF [4,5]. Skrabal et al. [6] used ECG detection combined with bio-impedance measurement technique to diagnose CHF. However, ECG can only detect the cardiac chronotropic and dromotropic action instead of the cardiac inotropic action that is reduced significantly in CHF patients [7], so it can be seen that single ECG detection for the diagnosis of CHF is insufficient.

Heart sound is very important as it directly reflects the mechanical properties of heart activity [8,9]. The studies on the relationship between heart sound and cardiac contractility indicate that the amplitude of the first heart sound (S1) is positively correlated with the maximum rise rate of left ventricular pressure ($r = 0.9551$, $p < 0.001$) and the amplitude of S1 is also closely related to the strength of cardiac contractility [10,11]. This has suggested that the amplitude of S1 can reflect the level of cardiac contractility. The most important aspect of cardiac dysfunction in heart failure is not the depressed cardiac performance observed at basal resting state but rather the loss of cardiac reserve (CR) [12,13], which is manifested in the decrease of cardiac contractility, so the detection and analysis of heart sound and the measurement of CR could provide important clues for the diagnosis of CHF. Based on the relationship between heart sound and cardiac contractility, an noninvasive and quantitative method for the assessment of CR has been proposed by our group [14,15]. Some diagnostic techniques such as real-time transmission of the phonocardiogram (PCG) through the Internet and computer-assisted auscultation were developed [16,17]. The application of CR indexes in monitoring and evaluating heart function for gestational woman was implemented [18]. However, until now, the studies about the application of CR in the diagnosis of CHF have not been reported, and the utilizations of heart sound characteristics for the diagnosis of CHF are few, except that an appearance of the third heart sound is regard as a highly specific and none sensitive marker for the diagnosis of CHF [19,20].

In this paper, an intelligent diagnosis system for CHF diagnosis was proposed, the schematic of which is shown in Fig. 1. It consists of acquisition system (hardware) and decision support system (software). The acquisition system includes sensor, acquisition circuit and computer device shown in Fig. 2. The decision support system is embedded in the computer. This paper emphatically introduces the decision support system that includes the following parts. The preprocessing is implemented based on amplitude normalization and modified wavelet packet denoising methods. The CR indexes such as the ratio of diastolic to systolic duration (D/S) and the amplitude ratio of the first to second heart sound (S1/S2) combined with three heart sound characteristics such as the frequency corresponding to the maximum peak of the normalized PSD curve (f_{PSDmax}), adaptive sub-band energy fraction (sub_EF) and multifractal spectrum parameter were proposed to structure a diagnostic feature set. The self-developed cardiac reserve monitor software (CRM version1.0, Chongqing University and Bo-Jing Medical Informatics Institute, China) was used to measure the CR indexes, and the heart sound characteristics were extracted based on maximum entropy spectra estimation (MESE), empirical mode decomposition (EMD) and multifractal detrended fluctuation analysis (MF-DFA) methods which are good at the analysis of non-stationary and non-linear physiological signal [21–23]. The LS-SVM was determined as the classifier of proposed system by the comparison of performances with back-propagation artificial neural network (BP-ANN) and hidden markov model

Fig. 2 – Cardiac reserve monitor used in this study.

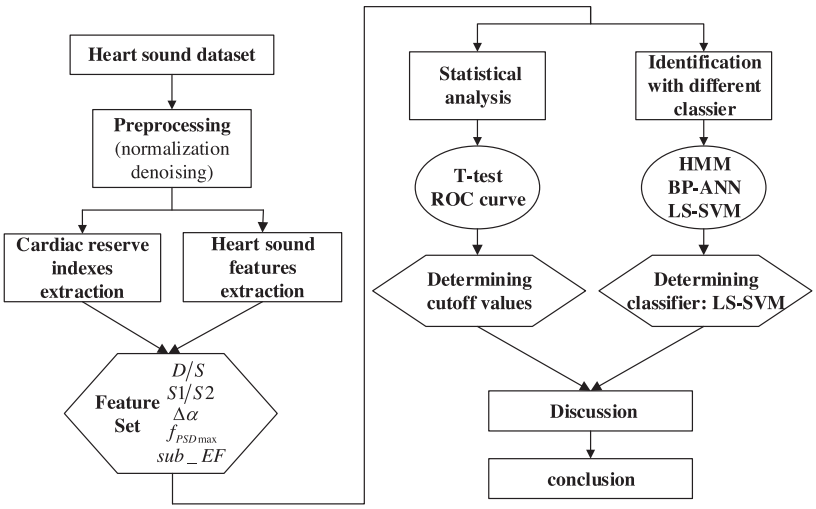

Fig. 3 – The structure diagram of the methodology in this paper.

(HMM). A dataset collected from the healthy volunteers and CHF patients was used to verify the proposed system. In addition, statistical analysis methods such as *t*-test and ROC curve were conducted to suggest the diagnosis thresholds. The purpose of our study is to explore a new effective computer-assisted diagnosis technique for the diagnosis of CHF.

The outline of this paper is organized as follows. Section 2 describes the detail of proposed diagnostic system including the methodologies of preprocessing, feature extraction and identification. Section 3 represents the statistical result of CR indexes and heart sound characteristics and the comparison of diagnostic performance among LS-SVM, BP-ANN and HMM. Section 4 discusses the differences of diagnostic indexes and characteristics between the healthy and CHF patients as well as the advantage and limitation of the proposed system. Section 5 gives the conclusion and future work of the study. The methodology framework of this paper is shown in Fig. 3.

2. Subjects and methodologies

2.1. *Study participants and clinic trial description*

The subjects consist of 88 healthy volunteers (college students and teachers) as controls and 64 CHF patients, who knew and signed the informed consent forms. The patients with CHF include the patients with heart failure with reduced ejection fraction (HFrEF) and heart failure with preserved ejection fraction (HFpEF), which are confirmed by the experienced cardiologists. The CHF patients with left ventricular ejection fraction (LVEF) more than 50% are considered as the patients with HFpEF, and the others are considered as the patients with HFrEF [24], shown in Table 1. LVEF was calculated by the modified Simpson's rule through echocardiography examine using a color Doppler Ultrasound medical machine (Vivid-7, GE company, USA). One minute heart sound was recorded from the apex position of each subject in rest state by employing the self-developed cardiac reserve monitor (11,025 Hz sampling frequency and 8-bit resolution) shown in Fig. 2. The normal and pathological heart sound samples were gathered at Chongqing University and the First and the Second Affiliated Hospitals of Chongqing University of Medical Sciences, respectively.

2.2. *Heart sound and CR*

The CR indexes such as S1/S2 and *D*/*S* were employed to evaluate cardiac function noninvasively [14], which denote the amplitude ratio of the first to the second heart sound (S2) and the ratio of diastolic to systolic duration in a cardiac cycle, illustrated in Fig. 4. The S1/S2 and *D*/*S* indexes are relative indicators used to evaluate the cardiac contractility reserve

Table 1 – The information of subjects enlisted in this study.

Subjects	Sex	Total	Type	Age
Healthy volunteers	Male $N=44$ Female $N=40$	88		Aged 18–60 (mean age, 35.64 ± 7.52 years)
CHF patients (without heart valve disorders)	Male $N=36$ Female $N=28$	64	HFrEF patients (Ejection fraction < 50%) $N=33$ HFpEF patients (Ejection fraction > 50%) $N=31$	Aged 38–70 (mean age, 61.56 ± 9.73 years)

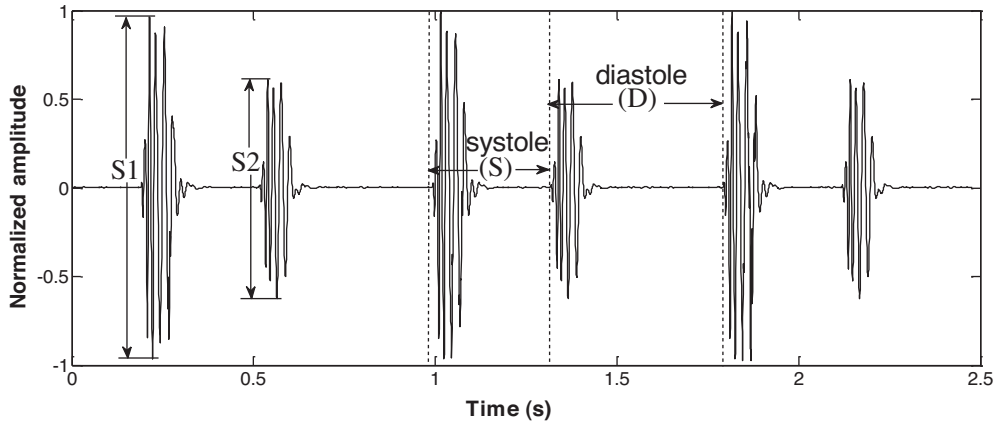

Fig. 4 – The illustration of cardiac reserve indexes.

which can reflect the relationship between left ventricular systolic function and peripheral circulation and appraise whether cardiac blood perfusion time is sufficient or not during diastole, respectively [15]. The CR indexes were measured by CRM software shown in Fig. 5.

2.3. *Data preprocessing*

Normalization is necessary to eliminate the amplitude differences of heart sound signals caused by the different chest wall thickness of subjects. It aims to maintain the amplitudes of the normalized heart sound signals from −1 to 1, and is operated as:

$$s_{norm}(n) = \frac{s(n)}{\max_{n=1}^{N}(|s(n)|)} \quad (1)$$

where N is the number of data points. $s(n)$ and $s_{norm}(n)$ are the original and normalized heart sound signal, respectively.

It is necessary to reduce the disturbance in heart sound singals that could cause great influence on the diagnosis performance [25]. Wavelet packet-based noise reduction has been proven effective to remove the disturbance introduced during the data gathering process such as the interferences of the background-noise, power and respiratory sounds [26]. In this study, we proposed a modified wavelet packet-based denoising method where the threshold estimation and calculation have been improved. Both the low and high frequency components of heart sound signal were decomposed to obtain the relevant approximate coefficients and detail coefficients by a Daubechies-10 wavelet at 8th level, and then the improved soft threshold model was employed to alter the detail

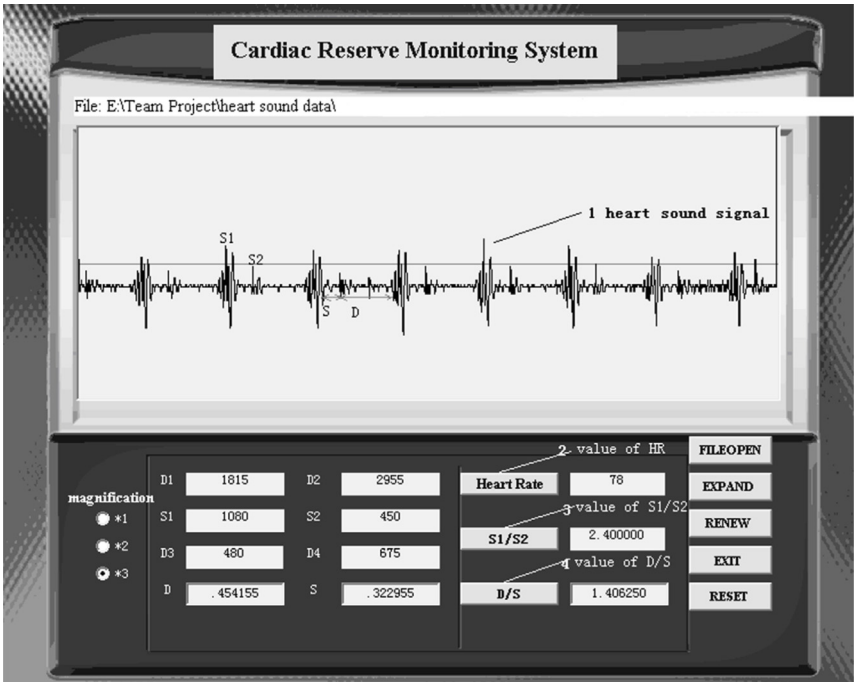

Fig. 5 – The CRM software graphical user interface: (1) a case of heart sound; (2) heart rate value; (3) S1/S2 value; (4) D/S value.

coefficients of each decomposition level, according to following principle:

$$\hat{\omega}_{j,k} = \begin{cases} th(\omega_{j,k}, \zeta_j), & \dfrac{|\omega_{j,k}|}{\zeta_j} \geq 1; \\ 0, & \dfrac{|\omega_{j,k}|}{\zeta_j} < 1; \end{cases} \tag{2}$$

$$th(\omega_{j,k}, \zeta_j) = \sin\ (\omega_{j,k})\sqrt{\omega_{j,k}^2 - \zeta_j^2} + \omega_{j,k} \tag{3}$$

$$\zeta_j = \frac{\sqrt{\ln N_j}}{\ln[e + (j-1)^2]} \tag{4}$$

where $\omega_{j,k}$ denotes the detail coefficients in the kth position of the jth decomposition level and ζ_j denotes the noise coefficient threshold in the jth decomposition level. $\widehat{\omega}_{j,k}$ is the modified detail coefficients. N_j is the number of the detail coefficients in the jth level. Finally, the reconstruction of the original approximate coefficients and improved detail coefficients was the heart sound signal after noise cancelation.

2.4. *Heart sound characteristics extraction*

2.4.1. *Multifractal spectrum*

Because of the superiority that differentiates between multifractal properties of the heart rate in the healthy people and patients with left ventricular systolic dysfunction [27], MF-DFA method, which implements an overall (localized or integral) multi-scale detection of multifractal behavior, proposed by Kantelhard et al. [28], was utilized to calculate the multifractal spectrum of heart sound correspondingly. Firstly, the sum of squares of deviations of $x(i)$ is computed as: $Y(j) = \sum_{i=0}^{j}(x(i) - \bar{x})$. And then, the new time series $Y(j)$ is divided into the non-overlapping equaling segments of size s (the number of these segments is $N_s = \mathrm{int}(N/s)$), which starts from both the beginning and end of the series to obtain $2N_s$ segments. The fluctuation $F^2(s, v)$ is calculated as the sum of squares of local differences:

$$\text{when}\quad v = 1, 2, \ldots, N_s, \quad F^2(s, v) \equiv \frac{1}{s}\sum_{i=1}^{s}[Y((v-1)s + i) - P_v(j)]^2 \tag{5}$$

$$\text{when}\quad v = N_s + 1, N_s + 2, \ldots, 2N_s, \quad F^2(s, v) \equiv \frac{1}{s}\sum_{i=1}^{s}[Y(N - (v - N_s)s + i) - P_v(j)]^2 \tag{6}$$

where s describes scale, $v \in [1, 2N_s]$ is the current segment number, $P_v(j)$ is the least-square fit within a segment v. The fluctuation function is determined as follows:

$$F_q(s) \equiv \left\{\frac{1}{2N_s}\sum_{v=1}^{2N_s}[F^2(s, v)]^{q/2}\right\}^{1/q} \tag{7}$$

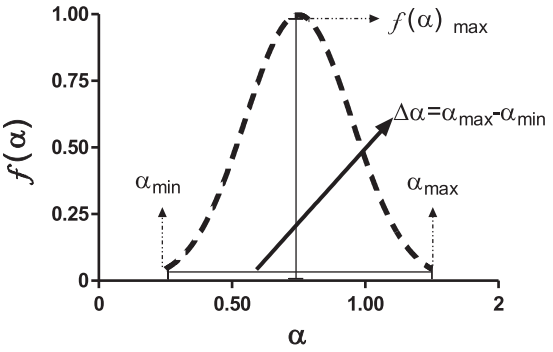

Fig. 6 – The illustration of multifractal spectrum.

where q is the fluctuation parameter, which allows us to focus the analysis upon different magnitudes of the overall fluctuations.

The power-law scaling function determines the scaling behavior of the fluctuation functions by analyzing the log–log plot of $F_q(s)$ versus s for each value of q, which is estimated in the form:

$$F_q(s) \sim s^{h(q)} \tag{8}$$

where $h(q)$ is the slope in a log–log plot of $F_q(s)$ versus s called generalized Hurst exponent. Finally, applying the Legendre transform to $h(q)$, we can get: $\alpha = h(q) + qh'(q)$ and $f(\alpha) = q[\alpha - h(q)] + 1$, and the multifractal spectrum $f(\alpha) \sim \alpha$ can be obtained. The multifractal spectrum parameters are illustrated in Fig. 6.

2.4.2. *Normalized power spectral density*

MESE with the advantage of high resolution and sidelobe suppression was selected to calculate the power spectral density (PSD) curve [29], defined by the Wiener–Khintchine theorem as the Fourier transform of the self-correlation function $R_x(m)$ of the original time series:

$$s_x(f) = \sum_{m=-\infty}^{\infty} R_x(m)e^{-j2\pi fmT} \tag{9}$$

According to the maximum entropy principle, let $\partial h/\partial R_x(m) = 0$, $|m| \geq M + 1$, we can obtain:

$$\int_{-f_c}^{f_c} \frac{e^{-j2\pi fmT}}{\hat{S}_x(f)}df = 0, \quad |m| \geq M + 1 \tag{10}$$

where $h = \lim_{m\to\infty}(H/m + 1) = \lim_{m\to\infty}(1/2)\log_{10}\det[R_x(m)]^{1/m+1}$ and $(1/\hat{S}_x(f)) = \sum_{n=-M}^{M} a_n e^{-j2\pi fnT}$, then the self-correlation function can be expressed as follows:

$$R_x(m) = \frac{f_c}{j\pi}\oint \frac{z^{m-1}}{\sum_{n=-M}^{M} a_n z^{-n}}dz, \quad 0 \leq m \leq M \tag{11}$$

According to the definition of PSD, the MESE-based PSD estimation is given by:

$$\hat{S}_x(f) = \frac{P_M}{2f_c|1 + \sum_{m=1}^{M} a_m e^{-j2\pi m f T}|^2} \tag{12}$$

where $P_M = 2f_c\sigma^2 T$, which is prediction error power. f_c is band width of the signal. a_m, σ^2 and T denote coefficients, the variance of the driving noise input and sampling period, respectively. In our study, the model order $m = 12$ was selected based on the criterion autoregressive transfer function proposed by Parzen [30].

2.4.3. *Adaptive sub-band energy fraction*

EMD technique developed by Huang et al. [31] is an adaptive method that can break down any nonlinear or nonstationary time series such as biomedical signals into a number of amplitude and frequency modulated components each called intrinsic mode function (IMF). Unlike Fourier and wavelet-based analysis methods, EMD does not require any a priori known basis function and is widely used to analyze biomedical signals. The signal can be expressed using IMFs as follows:

$$x(i) = \sum_{n=1}^{N} c_n(i) + r_N(i) \tag{13}$$

where N is the number of IMFs. $c_n(i)$ represents IMF and $r_N(i)$ is the residue after the decomposition of original signal. The algorithm flow chart of EMD is described in Fig. 7. The aim of EMD is to decompose a signal into a sum of adaptive bandwidth IMFs based on the adaptively defined basis functions with well-defined frequency localization levels. Then, we obtain the correlation between each IMF and the original signal $x(i)$ by computing the Pearson's correlation coefficient as follows:

$$r = \frac{\sum_{i=1}^{n}(x_i - \bar{x})(y_i - \bar{y})}{\sqrt{\sum_{i=1}^{n}(x_i - \bar{x})^2 \cdot \sum_{i=1}^{n}(y_i - \bar{y})^2}} \tag{14}$$

where x_i and y_i denote the discrete points of the original signal $x(i)$ and the IMF, respectively.

Then, the special IMFs with a value of r more than 0.1 were selected for the calculation of adaptive *sub_EF*. According to Parseval theorem [32], the energy spectrum of the original signal can be computed as follows:

$$E = \int_{\Gamma} |x(i)|^2 dt = \sum_{i=1}^{N} |x(i)|^2 \tag{15}$$

where N is the number of sampling points of the discrete original signal. Similarly, the energy spectrum of the selected IMF is given as:

$$E = \int_{\Gamma} |c(i)|^2 dt = \sum_{i=1}^{N} |c(i)|^2 \tag{16}$$

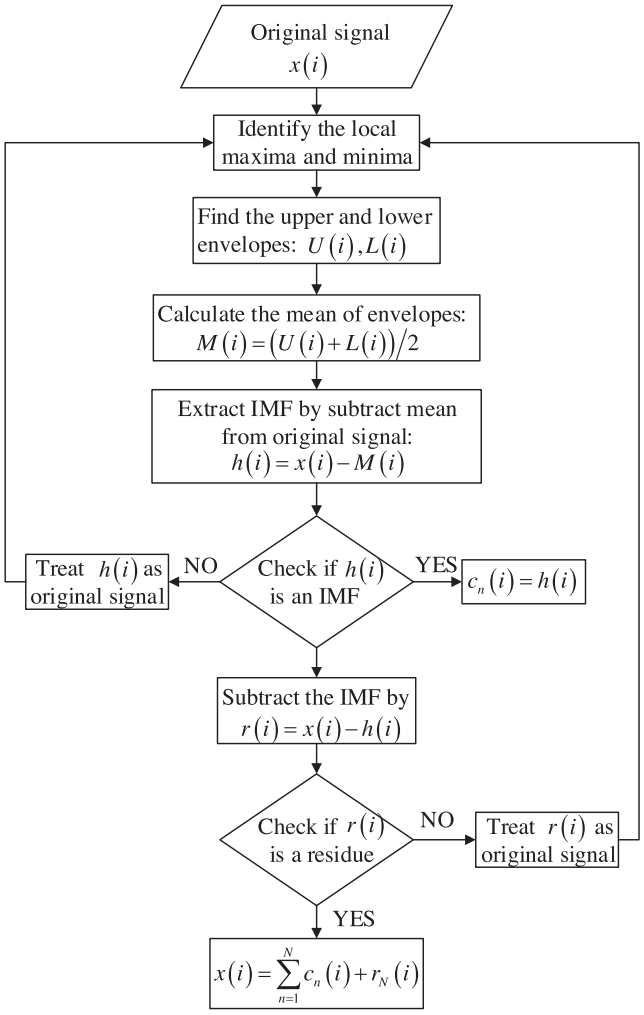

Fig. 7 – The flow diagram of EMD.

So the calculation of adaptive *sub_EF* refers to:

$$sub\_EF = \frac{\sum_{i=1}^{N}|c(i)|^2}{\sum_{i=1}^{N}|x(i)|^2} \tag{17}$$

In this study, we only select the first five IMFs to calculate adaptive *sub_EFs*.

2.5. *LS-SVM-based intelligent diagnosis system*

LS-SVM method firstly proposed by Suykens and Vandewalle [33] is an effective approch especially to solve the problems of prediction and classification on artificial intelligence. It solves a set of linear equations so as to avoid solving high-computational-cost quadratic programming problem [34]. By using an appropriate kernel function (KF), LS-SVM maps the input data into a high dimensional state space where an optimal separating hyperplane can separate the different classes linearly. A training set of input data $\{x_i\}_{i=1}^{N}$ and output data $\{y_i\}_{i=1}^{N}$ are given where $x_i \in \Re^n$ and $y_i \in \Re$ represent the ith input

and output patterns. The hyperplane separating the input data in the state space can be expressed by Eq. (18)

$$\omega^T x + b = 0 \tag{18}$$

The regression function can be given as

$$y(x) = \omega^T x + b \tag{19}$$

The output of LS-SVM is constructed so that the optimal hyperplane satisfies the following constraint.

$$\omega^T \psi(x_i) + b \geq +1 - \xi_i \quad \text{for} \quad y_i = +1 \tag{20}$$

$$\omega^T \psi(x_i) + b \leq -1 + \xi_i \quad \text{for} \quad y_i = -1 \tag{21}$$

These are equivalent to

$$y_i[\omega^T \psi(x_i) + b] \geq 1 - \xi_i, \quad i = 1, 2, \ldots, N \tag{22}$$

where $\psi(\cdot)$ represents a function mapping the inputs into the state space, ω represents a weight vector which defines the boundary, b is a bias, ξ_i is the nonnegative slack variable which controls the constraint violation and makes the training error minimum.

The discriminant boundary is determined by maximizing the margin among all hyperplanes, therefore the LS-SVM classifiers is defined by minimizing the following equation:

$$\min_{\omega, b, \xi} \Phi(\omega, b, \xi) = \frac{1}{2}\omega^T \omega + \frac{1}{2}\gamma \sum_{i=1}^{N} \xi_i^2 \tag{23}$$

$$\text{Subject to} \quad y_i[\omega^T \psi(x_i) + b] = 1 - \xi_i, \quad i = 1, 2, \ldots, N \tag{24}$$

where γ is a penalty parameter which controls the trade-off of training errors.

To solve the optimization problem, the Lagrangian function has been constituted by introducing Lagrange multipliers α_i

$$L(\omega, b, \xi; \alpha) = \Phi(\omega, b, \xi) - \sum_{i=1}^{N} \alpha_i \{y_i[\omega^T \psi(x_i) + b] - 1 + \xi_i\} \tag{25}$$

According to the Kuhan–Tucker conditions, we can obtain [33,35]:

$$\frac{\partial L}{\partial \omega} = 0 \Rightarrow \omega = \sum_{i=1}^{N} \alpha_i y_i \psi(x_i) \tag{26}$$

$$\frac{\partial L}{\partial b} = 0 \Rightarrow \sum_{i=1}^{n} \alpha_i y_i = 0 \tag{27}$$

$$\frac{\partial L}{\partial \xi_i} = 0 \Rightarrow \alpha_i = \gamma \xi_i \tag{28}$$

$$\frac{\partial L}{\partial \alpha_i} = 0 \Rightarrow y_i[\omega^T \psi(x_i) + b] - 1 + \xi_i = 0 \tag{29}$$

$i = 1, 2, \ldots, N$

Table 2 – The structure description of HMM, BP-ANN and LS-SVM classifiers.

Classifier	Structure description
HMM	4 states and 13 Gaussian mixtures
BP-ANN	3 layers, 5 input, 20 hidden layers and 2 output
LS-SVM	$\gamma = 5$, $\theta = 0.4$ and $\xi_i = 0.01$

Finally, the LS-SVM classifier model is constructed by

$$y(x) = \sum_{i=1}^{N} \alpha_i K(x, x_i) + b \tag{30}$$

where $K(x, x_i)$ is the KF. In literatures, some widely used KFs includes linear, polynomial, sigmoid and Gaussian radial basis function (GRBF). In this study, the GRBF shown in Eq. (31) as the KF of LS-SVM was employed for the intelligent diagnosis of CHF, which has been proven more effective in previous work [26].

$$K(x, x_i) = \exp\left(\frac{-||x - x_i||^2}{2\theta^2}\right) \tag{31}$$

where θ is the kernel parameter that affects the structure of feature vector. In calculation, both γ and θ values were chosen empirically to achieve a satisfactory performance of the system, represented in the last column of Table 2.

2.6. *Statistical analysis*

The statistical results of heart sound characteristics and CR indexes were expressed as mean ± standard deviation. Student's *t*-test was implemented to analyze whether statistical differences of those exist between the control and CHF groups. A value of p less than 0.05 was considered as a statistical difference. ROC curve analysis was used to select the diagnosis thresholds for distinguishing the control from CHF groups. The area under the ROC curve (AUC) was employed as a performance measurement for the supervised classification in this study. The statistical analysis was performed by SPSS software (version 18.0) [36].

3. Results

3.1. *The analysis result of CR indexes and heart sound characteristics*

LVEF is a worldwide acknowledged index to reflect the differences of heart pump function between the healthy and people with CHF [37]. It was just used to verify the diagnosis of CHF in this study. CR indexes extracted from the healthy volunteers and CHF patients are listed in Table 3. The *D*/*S* and *S*1/*S*2 values of control group are higher than those of CHF group, while the HR values of the control group are lower.

Table 4 presents the calculated results of multifractal spectrum parameters. The width of multifractal spectrum $\Delta\alpha$, which is related to the degree of multifractality [3], is obtained by calculating the distance between the α values in the starting

Table 3 – The results of clinic trial including cardiac reserve and cardiac function indexes.

Dataset	D/S	S1/S2	HR	LVEF
Control group (N = 88)	1.72 ± 0.31	1.79 ± 0.69	75.27 ± 11.87	62.25 ± 3.56
CHF group (N = 64)	1.37 ± 0.19	1.56 ± 1.03	88.78 ± 12.5	51.05 ± 6.99

Table 4 – The multifractal spectrum parameters for control versus CHF group.

Dataset	α_{min}	α_{max}	$\Delta\alpha$	$f(\alpha)_{max}$
Control group (N = 88)	0.16 ± 0.05	1.59 ± 0.20	1.43 ± 0.19	1.00 ± 0.01
CHF group (N = 64)	0.39 ± 0.12	1.54 ± 0.16	1.15 ± 0.29	1.00 ± 0.01

Table 5 – The normalized PSD and sub-band energy fraction characteristics for control versus CHF.

Dataset	f_{PSDmax} (Hz)	IMF1 (%)	IMF2 (%)	IMF3 (%)	IMF4 (%)	IMF5 (%)
Control group (N = 88)	30.82 ± 3.23	4.13 ± 3.10	38.00 ± 9.88	22.73 ± 4.00	8.29 ± 3.49	1.01 ± 0.81
CHF group (N = 64)	24.97 ± 4.13	3.06 ± 1.36	31.14 ± 5.93	27.32 ± 3.36	15.37 ± 3.80	2.47 ± 1.96

and ending points of the curve shown in Fig. 6. Compared to the CHF group, the heart sounds from the control group with a larger $\Delta\alpha$ have a stronger degree of multifractality.

Fig. 8 shows the normalized PSD curves of heart sounds for a healthy subject (left panel) and CHF patient (right panel). It is found that the normalized PSDs of both groups are distributed concentratedly on the low frequency range of less than 150 Hz. The calculated results of f_{PSDmax} and *sub_EF*s are listed in Table 5. For the control group, the average f_{PSDmax} is 30.82 ± 3.23 Hz, which is higher than that of the CHF group. It is also found that the distributions of the adaptive *sub_EF*s of the heart sounds from the two groups are similar and the biggest *sub_EF* appear in the IMF2 for the control and CHF groups.

3.2. *The experimental result of CHF diagnosis*

A dataset consisting of 152 heart sound samples was used to evaluate the diagnostic performance of the proposed technique, and it is divided equally into the training and testing sets. The average classification accuracy obtained from the double-fold cross validation was taken as the diagnostic accuracy. The feature vector set consisting of the CR indexes and heart sound characteristics described in Table 6 was used as the input of LS-SVM for the intelligent diagnosis. To verify the effectiveness of the proposed system, the diagnostic performance of the LS-SVM-based proposed system has been compared with that of BP-ANN and HMM -based methods. The selected structures for HMM, BP-ANN and LS-SVM are shown in Table 2. The performance comparison of the systems with different classifier is represented in Table 7. It is noted that the proposed system achieves 95.39% diagnostic accuracy, 96.59% sensitivity and 93.75% specificity which are 11.18%, 11.36% and 10.94% higher than BP-ANN-based system and 13.80%, 13.64% and 14.07% higher than HMM-based system.

Table 6 – The diagnostic feature set used in our study.

Feature	Definition
D/S	The ratio of diastolic to systolic duration
S1/S2	The ratio of the amplitude of the first heart sound to that of the second heart sound
$\Delta\alpha$	The width of multifractal spectrum
f_{PSDmax}	The frequency corresponding to the maximum peak of the normalized PSD curve
sub_EF	Adaptive sub-band energy fraction

3.3. *The statistical result*

The t-test result of CR indexes, cardiac function indexes and heart sound characteristics are vividly described by histogram in Fig. 9, which are statistically significant ($p < 0.05$). ROC curves analysis provides selected cutoff values for each significant feature parameter such as *D/S*, S1/S2, $\Delta\alpha$ and f_{PSDmax}, which could be employed as reference diagnosis threshold for the

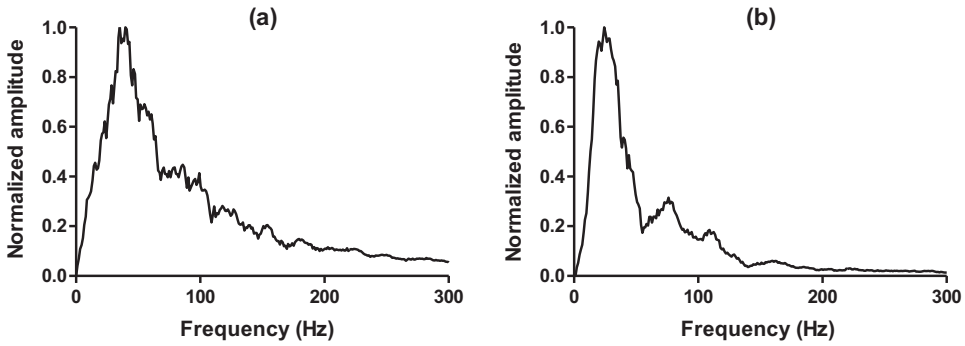

Fig. 8 – The normalized PSD curves of heart sounds for (a) a healthy subject and (b) a patient with CHF.

Table 7 – The performance comparison of the systems with different classifier.

Classifier type	Input dataset	Classification result			
		Output	Accuracy (%)	Sensitivity (%)	Specificity (%)
HMM	Control = 88 CHF = 64	Control = 73 CHF = 51	81.58	82.95	79.68
BP-ANN	Control = 88 CHF = 64	Control = 75 CHF = 53	84.21	85.23	82.81
LS-SVM	Control = 88 CHF = 64	Control = 85 CHF = 60	95.39	96.59	93.75

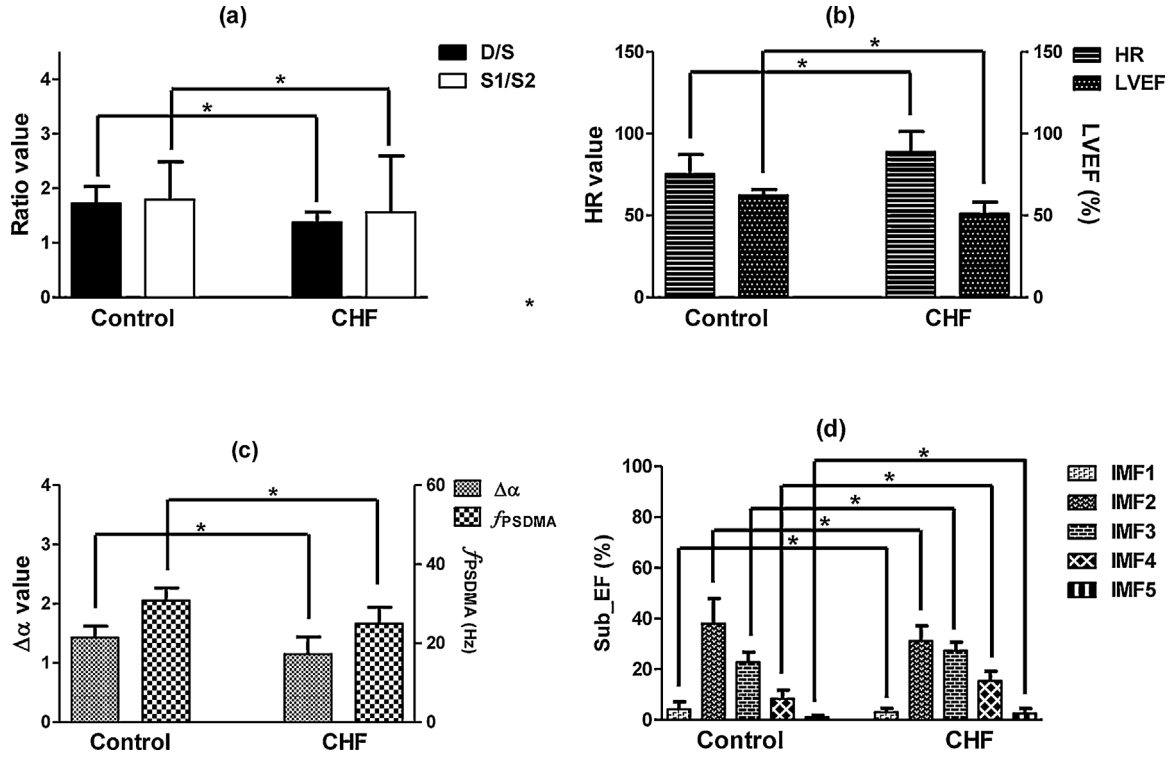

Fig. 9 – The histogram with t-test result of the CR indexes, cardiac function indexes and heart sound characteristics; (a) *D/S* and *S1/S2* value, (b) HR and LVEF value, (c) $\Delta\alpha$ value and f_{PSDmax} and (d) *sub_EF* in each IMF.

cardiologists to verify the automatic diagnosis result. It is shown in Fig. 10 that the selected cutoff values with the best sensitivity and specificity for the identification of CHF were determined by Youden index ($J = sensitivity\% + specificity\% - 1$). The corresponding result was summarized in Table 8. AUC as a common indicator of quality measures the degree of accuracy in the ROC curve analysis. The *p* value shows the ability of each feature parameter to discriminate the control from CHF groups. The smaller the *p* value is, the better the performance of ROC curve is.

4. Discussion

4.1. *The differences of CR indexes between the control and CHF group*

Cardiac reserve is regarded as an important physiological function base of the fitness and exercise performance of human beings [38]. This paper has investigated the differences of CR indexes between the healthy and CHF patients. *D/S* value

Table 8 – The results of ROC curve analysis for control versus CHF group.

Control versus CHF	AUC	Standard error of AUC	95% Confidence interval	*P*-value	Selected cutoff values
D/S	0.8267	0.03624	0.7557–0.8978	0.0001	1.59
S1/S2	0.6498	0.04442	0.5627–0.7369	0.0009	1.31
$\Delta\alpha$	0.8002	0.04389	0.7142–0.8862	0.0001	1.34
f_{PSDmax}	0.8465	0.04094	0.7662–0.9267	0.0001	22.46 Hz

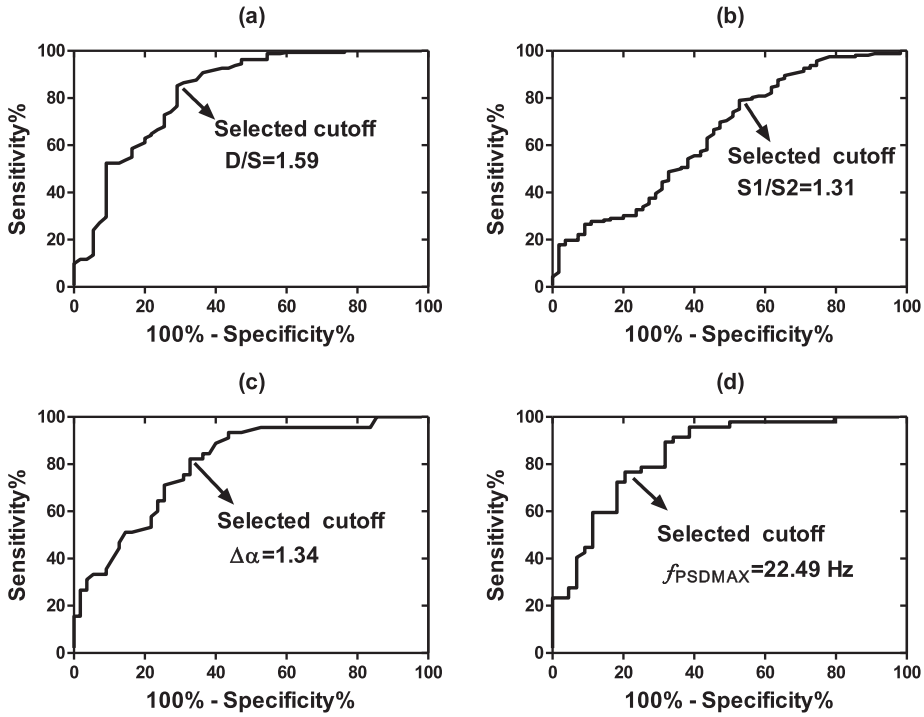

Fig. 10 – The ROC curves of the control versus CHF group; (a) *D/S* value, (b) S1/S2 value, (c) $\Delta\alpha$ value and (d) f_{PSDmax}.

is the time index of heart perfusion reserve, and it emphasizes the significance of the appropriate ratio of diastole to systole duration to maintain the healthy function of heart pump [15]. Because the most part of coronary blood flow occurs during the diastole of each cardiac cycle [39], higher *D/S* denotes a healthy myocardial perfusion status. However, CHF could result in either the left ventricular diastolic or systolic dysfunction so that the left ventricular filling is insufficient and myocardial blood flow perfusion reduces, thus the CHF group has a lower *D/S* values than control group in the rest state. S1/S2 reflects cardiac contractility reserve. It has been proven that the amplitudes of S1 and S2 are closely related to cardiac contractility and the peripheral resistance, respectively [11,40]. In the condition of CHF, the heart with a malfunction of pump function cannot transport abundant rich-oxygen blood to ensure the need of peripheral tissues, and it manifests a reduction of cardiac contractility during systole of each cardiac cycle. The blood stroke with a smaller kinetic energy could suffer from a greater peripheral resistance compared to the healthy condition. As a result, the S1/S2 values of the CHF group are decreased compared to control group. Furthermore, the decreased S1/S2 is also observed in the patients with left ventricular systolic dysfunction [41]. This report can support the result we obtained.

4.2. *The differences of heart sound characteristics between control and CHF group*

To our knowledge, this paper is the first report on multifractal analysis of heart sounds collected from the healthy people and CHF patients. Furthermore, the multifractal nature of heart sound has only been utilized to distinguish prolapsed mitral valve from healthy heart [42], and few studies on multifractal analysis of heart sound have been reported so far. The existence of multifractal spectrum demonstrates the evidence of multifractality in the heart sounds from healthy people and CHF patients. According to the relationship between $\Delta\alpha$ and the degree of multifractality [3], we have discovered that the multifractal nature has a loss in the heart sounds of CHF patients, and the same loss can be found in ECG and heartbeat interval series of the CHF patient [1,3]. It is because that the changes of myocardial mechanical properties caused by CHF could influence cardiac electrophysiology directly by the process of mechano-electric feedback [43].

The shapes of normalized PSD curves and f_{PSDmax} values of the CHF and control groups are discrepant due to the different cardiac hemodynamic process. The *sub_EF*s show that the energy distribution of heart sound concentrates mainly on the low frequency component, which is be similar to the spectral distribution that main frequency range of heart sound focus on S1 and S2 [44,45]. Although the biggest *sub_EF* appears in the IMF2 for the control and CHF groups, the *sub_EF*s of the control group in IMF1 and IMF2 are higher while in IMF3, IMF4 and IMF5 they are lower, compared to those of the CHF group. This indicates the signal energy distribution of heart sounds from the CHF patients mainly concentrates IMF2, IMF3 and IMF4 while that of the control group just concentrates IMF2 and IMF3. The reason could be that the reduced intensity of S1 caused by depressed cardiac contractility leads to the decreased percentage of S1 energy fraction.

4.3. *The advantage and limitation of our proposed system*

The advantages of our system are found in two aspects such as the choices of diagnosis characteristics and classifier. Firstly,

the diagnosis features consist of CR indexes and heart sound characteristics, which can not only contain the physiological and pathological information in cardiac activity but also reflect the differences of heart sound signals in morphology, time-frequency domain and energy. This is different from the reports referring to heart sound feature extraction [22,46,47]. Secondly, the selected LS-SVM classifier is superior to BP-ANN and HMM in this study. It is mainly shown in the following aspects: the LS-SVM costs a shorter training time for reaching an optimum structure [48]. The LS-SVM was trained based on a convex optimization problem so as to be estimated a global solution, but the BP-ANN cannot reach one global solution due to the initial weights are randomly selected [49,50]. The LS-SVM also can avoid suffering from local minimum mistakes and the overfitting more successfully than BP-ANN and HMM [51]. Finally, the result of contrast experiment shown in Table 7 indicates the performance of LS-SVM is better than that of BP-ANN and HMM. As a result, our proposed system with LS-SVM classifier has the advantage of simple structure, global optimum and strong generalization ability. In this study, we did not consider the subjects with heart murmurs, so if a heart sound sample with murmurs was input the system, the methodology would report misclassification. However, the shortcoming will be solved by training the classifier with the corresponding dataset. In the future, different categories of sample examples will be used to train the classifier so as to improve the diagnosis performance. The proposed intelligent diagnosis system applied to the diagnosis of multiple diseases is an important and worthwhile research subject, and large sample data need to be collected to train the diagnosis model. This is also the main research direction in our future work in spite of challengeable work.

5. Conclusion

In this paper, we proposed an intelligent system for the diagnosis of CHF based on LS-SVM. The CR indexes such as D/S and $S1/S2$ and heart sound characteristics such as $\Delta\alpha$, $f_{PSD\max}$ and adaptive sub_EF are constituted diagnosis features as the input of classifier. A dataset collected from the healthy volunteers and CHF patients was used to verify the proposed system. The LS-SVM classifier with satisfactory accuracy, sensitivity and specificity was selected through the comparison with BP-ANN and HMM. In addition, student's t-test was performed to examine the difference of each diagnosis feature between the two groups. The ROC curve analysis was used to determine the selected cutoff values for CHF identification, which suggests the CR indexes and heart sound characteristics as auxiliary diagnostic indicators could be supplement for CHF diagnosis. To our knowledge, this is also the first study on the analysis of the heart sounds applied to the diagnosis of CHF.

In the future, the planning work should involve the following aspects. More samples should be investigated to establish a diagnosis model for CHF. The physiological significance corresponding to the changes of indexes should be explored in great depth. The ultimate purpose is to popularize the useful indexes in clinical application. This study suggests that heart sound could provide effective clues for the diagnosis of CHF.

Conflict of interest statement

None.

Acknowledgement

This study is supported by the National Natural Science Foundation of China (No. 30770551).

REFERENCES

[1] P.C. Ivanov, L.A.N. Amaral, A.L. Goldberger, S. Havlin, M.G. Rosenblum, Z.R. Struzik, H.E. Stanley, Multifractality in human heartbeat dynamics, Nature 399 (1999) 461–465.
[2] P.C. Ivanov, L.A. Nunes Amaral, A.L. Goldberger, S. Havlin, M.G. Rosenblum, H.E. Stanley, Z.R. Struzik, From 1/*f* noise to multifractal cascades in heartbeat dynamics, Chaos 11 (2001) 641–652.
[3] S. Dutta, Multifractal properties of ECG patterns of patients suffering from congestive heart failure, J. Stat. Mech.: Theory Exp. 2010 (2010) P12021.
[4] A. Kashani, S.S. Barold, Significance of QRS complex duration in patients with heart failure, J. Am. Coll. Cardiol. 46 (2005) 2183–2192.
[5] Z.M. Zhang, P.M. Rautaharju, R.J. Prineas, L. Loehr, W. Rosamond, E.Z. Soliman, Usefulness of electrocardiographic QRS/T angles with versus without bundle branch blocks to predict heart failure (from the Atherosclerosis Risk in Communities Study), Am. J. Cardiol. 114 (2014) 412–418.
[6] F. Skrabal, G.P. Pichler, G. Gratze, A. Holler, Adding hemodynamic and fluid leads to the ECG. Part I: the electrical estimation of BNP, chronic heart failure (CHF) and extracellular fluid (ECF) accumulation, Med. Eng. Phys. 36 (2014) 896–904 (discussion 896).
[7] F. Triposkiadis, G. Karayannis, G. Giamouzis, J. Skoularigis, G. Louridas, J. Butler, The sympathetic nervous system in heart failure: physiology, pathophysiology, and clinical implications, J. Am. Coll. Cardiol. 54 (2009) 1747–1762.
[8] C. Wu, B.A. Herman, S.M. Retta, L.W. Grossman, J.-S. Liu, N.H.C. Hwang, On the closing sounds of a mechanical heart valve, Ann. Biomed. Eng. 33 (2005) 743–750.
[9] H. Tang, C. Ruan, T. Qiu, Y. Park, S. Xiao, Reinvestigation of the relationship between the amplitude of the first heart sound to cardiac dynamics, Physiol. Rep. 1 (2013) e00053.
[10] M.L. Rice, D.J. Doyle, Comparison of phonocardiographic monitoring locations, in: 17th Annual Conference of the IEEE on Engineering in Medicine and Biology Society, 1995, pp. 685–686.
[11] P.B. Hansen, A.A. Luisada, D.J. Miletich, R.F. Albrecht, Phonocardiography as a monitor of cardiac performance during anesthesia, Anesth. Analg. 68 (1989) 385–387.
[12] L. Tan, Cardiac pumping capability and prognosis in heart failure, Lancet 328 (1986) 1360–1363.
[13] H.S. Norman, J. Oujiri, S.J. Larue, C.B. Chapman, K.B. Margulies, N.K. Sweitzer, Decreased cardiac functional reserve in heart failure with preserved systolic function, J. Card. Fail. 17 (2011) 301–308.
[14] S. Xiao, X. Guo, X. Sun, Z. Xiao, A relative value method for measuring and evaluating cardiac reserve, Biomed. Eng. Online 1 (2002) 6.
[15] S. Xiao, X. Guo, F. Wang, Z. Xiao, G. Liu, Z. Zhan, X. Sun, Evaluating two new indicators of cardiac reserve, Eng. Med. Biol. Mag. IEEE 22 (2003) 147–152.
[16] R.L. Watrous, W.R. Thompson, A. SJ, The impact of computer-assisted auscultation on physician referrals of

asymptomatic patients with heart murmurs, Clin. Cardiol. 31 (2008) 79–83.
[17] Z. Guo, C. Moulder, Y. Zou, M. Loew, D. LG, A virtual instrument for acquisition and analysis of the phonocardiogram and its internet-based application, Telemed. e-Health 7 (2001) 333–339.
[18] X. Guo, X. Ding, M. Lei, M. Xie, L. Zhong, S. Xiao, Non-invasive monitoring and evaluating cardiac function of pregnant women based on a relative value method, Acta Physiol. Hung. 99 (2012) 382–391.
[19] S.P. Collins, C.J. Lindsell, W.F. Peacock, V.D. Hedger, J. Askew, D.C. Eckert, A.B. Storrow, The combined utility of an S3 heart sound and B-type natriuretic peptide levels in emergency department patients with dyspnea, J. Card. Fail. 12 (2006) 286–292.
[20] G.M. Marcus, I.L. Gerber, B.H. McKeown, J.C. Vessey, M.V. Jordan, M. Huddleston, C.E. McCulloch, E. Foster, K. Chatterjee, A.D. Michaels, Association between phonocardiographic third and fourth heart sounds and objective measures of left ventricular function, JAMA 293 (2005) 2238–2244.
[21] M.J. Lewis, A.L. Short, J. Suckling, Multifractal characterisation of electrocardiographic RR and QT time-series before and after progressive exercise, Comput. Methods Programs Biomed. 108 (2012) 176–185.
[22] B.A. Reyes, S. Charleston-Villalobos, R. Gonzalez-Camarena, T. Aljama-Corrales, Assessment of time-frequency representation techniques for thoracic sounds analysis, Comput. Methods Programs Biomed. 114 (2014) 276–290.
[23] U.R. Acharya, O. Faust, V. Sree, G. Swapna, R.J. Martis, N.A. Kadri, J.S. Suri, Linear and nonlinear analysis of normal and CAD-affected heart rate signals, Comput. Methods Programs Biomed. 113 (2014) 55–68.
[24] R.S. Bhatia, J.V. Tu, D.S. Lee, P.C. Austin, J. Fang, A. Haouzi, Y. Gong, P.P. Liu, Outcome of heart failure with preserved ejection fraction in a population-based study, New Engl. J. Med. 355 (2006) 260–269.
[25] X. Cheng, Z. Zhang, Denoising method of heart sound signals based on self-construct heart sound wavelet, AIP Adv. 4 (2014) 1203–1209.
[26] Y. Zheng, X. Guo, X. Ding, A novel hybrid energy fraction and entropy-based approach for systolic heart murmurs identification, Expert Syst. Appl. 42 (2015) 2710–2721.
[27] R. Galaska, D. Makowiec, A. Dudkowska, A. Koprowski, K. Chlebus, J. Wdowczyk-Szulc, A. Rynkiewicz, Comparison of wavelet transform modulus maxima and multifractal detrended fluctuation analysis of heart rate in patients with systolic dysfunction of left ventricle, Ann. Noninvasive Electrocardiol. 13 (2008) 155–164.
[28] J.W. Kantelhardt, S.A. Zschiegner, E. Koscielny-Bunde, S. Havlin, A. Bunde, H.E. Stanley, Multifractal detrended fluctuation analysis of nonstationary time series, Phys. A: Stat. Mech. Appl. 316 (2002) 87–114.
[29] S.J. Johnsen, N. Andersen, On power estimation in maximum entropy spectral analysis, Geophysics 43 (2012) 681.
[30] E. Parzen, Multiple Time Series: Determining the Order of Approximating Autoregressive Schemes, DTIC Document, 1975.
[31] N.E. Huang, Z. Shen, S.R. Long, M.C. Wu, H.H. Shih, Q. Zheng, N.-C. Yen, C.C. Tung, H.H. Liu, The empirical mode decomposition and the Hilbert spectrum for nonlinear and non-stationary time series analysis, in: Proceedings of the Royal Society of London A: Mathematical, Physical and Engineering Sciences, The Royal Society, 1998, pp. 903–995.
[32] A.M. Gargoom, N. Ertugrul, W.L. Soong, Automatic classification and characterization of power quality events, IEEE Trans. Power Deliv. 23 (2008) 2417–2425.
[33] J.A. Suykens, J. Vandewalle, Least squares support vector machine classifiers, Neural Process. Lett. 9 (1999) 293–300.
[34] D. Tsujinishi, S. Abe, Fuzzy least squares support vector machines for multiclass problems, Neural Netw. 16 (2003) 785–792.
[35] M.A. Hanson, On sufficiency of the Kuhn–Tucker conditions, J. Math. Anal. Appl. 80 (1981) 545–550.
[36] D.T.L. Shek, C.M.S. Ma, Longitudinal data analyses using linear mixed models in SPSS: concepts, procedures and illustrations, Sci. World J. 11 (2011) 42–76.
[37] R.S. Vasan, S.M.G. Larson, E.J. Benjamin, J.C. Evans, C.K. Reiss, D. Levy, Congestive heart failure in subjects with normal versus reduced left ventricular ejection fraction: prevalence and mortality in a population-based cohort, J. Am. Coll. Cardiol. 33 (1999) 1948–1955.
[38] G. Cooke, P. Marshall, J. Al-Timman, D. Wright, R. Riley, R. Hainsworth, L. Tan, Physiological cardiac reserve: development of a non-invasive method and first estimates in man, Heart 79 (1998) 289–294.
[39] M. Abe, H. Tomiyama, H. Yoshida, N. Doba, Diastolic fractional flow reserve to assess the functional severity of moderate coronary artery stenoses comparison with fractional flow reserve and coronary flow velocity reserve, Circulation 102 (2000) 2365–2370.
[40] T. Bombardini, V. Gemignani, E. Bianchini, L. Venneri, C. Petersen, E. Pasanisi, L. Pratali, M. Pianelli, F. Faita, M. Giannoni, Arterial pressure changes monitoring with a new precordial noninvasive sensor, Cardiovasc. Ultrasound 6 (2008) 41.
[41] B.P. Hsieh, K. Unver, E. McNulty, N.B. Schiller, The amplitude ratio of the first to second heart sound is reduced in left ventricular systolic dysfunction, Int. J. Cardiol. 145 (2010) 133–135.
[42] A. Gavrovska, G. Zajic, I. Reljin, B. Reljin, Classification of prolapsed mitral valve versus healthy heart from phonocardiograms by multifractal analysis, Comput. Math. Methods Med. 2013 (2013) 376152.
[43] J. Dean, M. Lab, Arrhythmia in heart failure: role of mechanically induced changes in electrophysiology, Lancet 333 (1989) 1309–1312.
[44] H. Naseri, M.R. Homaeinezhad, Detection and boundary identification of phonocardiogram sounds using an expert frequency-energy based metric, Ann. Biomed. Eng. 41 (2013) 279–292.
[45] J.C. Wood, A.J. Buda, D.T. Barry, Time-frequency transforms: a new approach to first heart sound frequency dynamics, IEEE Trans. Biomed. Eng. 39 (1992) 730–740.
[46] S. Sun, H. Wang, Z. Jiang, Y. Fang, T. Tao, Segmentation-based heart sound feature extraction combined with classifier models for a VSD diagnosis system, Expert Syst. Appl. 41 (2014) 1769–1780.
[47] S. Choi, G.B. Jung, H.-K. Park, A novel cardiac spectral segmentation based on a multi-Gaussian fitting method for regurgitation murmur identification, Signal Process. 104 (2014) 339–345.
[48] S. Ari, K. Hembram, G. Saha, Detection of cardiac abnormality from PCG signal using LMS based least square SVM classifier, Expert Syst. Appl. 37 (2010) 8019–8026.
[49] E. Avci, A new intelligent diagnosis system for the heart valve diseases by using genetic-SVM classifier, Expert Syst. Appl. 36 (2009) 10618–10626.
[50] R. Moraes, J.F. Valiati, W.P.G. Neto, Document-level sentiment classification: an empirical comparison between SVM and ANN, Expert Syst. Appl. 40 (2013) 621–633.
[51] C. Cortes, V. Vapnik, Support-vector networks, Mach. Learn. 20 (1995) 273–297.